



Dalton  
Transactions

**Site-selective Halogenation of Mixed-valent Vanadium Oxide Clusters**

Journal:	<i>Dalton Transactions</i>
Manuscript ID	DT-ART-03-2020-001077.R1
Article Type:	Paper
Date Submitted by the Author:	12-Apr-2020
Complete List of Authors:	Maiola, Michela ; University of Rochester, Chemistry Petel, Brittney; University of Rochester, Chemistry Brennessel, William; University of Rochester, Department of Chemistry Matson, Ellen; University of Illinois at Urbana-Champaign, Chemistry

SCHOLARONE™  
Manuscripts

## ARTICLE

## Site-selective Halogenation of Mixed-valent Vanadium Oxide Clusters

Received 00th January 20xx,  
Accepted 00th January 20xx

Michela L. Maiola,<sup>a</sup> Brittney E. Petel,<sup>a</sup> William W. Brennessel,<sup>a</sup> and Ellen M. Matson<sup>\*a</sup>

DOI: 10.1039/x0xx00000x

Here, we expand on the synthesis and characterization of chloride-functionalized polyoxovanadate-alkoxide (POV-alkoxide) clusters, to include the halogenation of mixed-valent vanadium oxide assemblies. These findings build on our previously disclosed results describing the preparation of a mono-anionic chloride-functionalized cluster,  $[V_6O_6Cl(OC_2H_5)_{12}]^{1-}$ , by chlorination of  $[V_6O_7(OC_2H_5)_{12}]^{2-}$  with  $AlCl_3$ , aimed at understanding the electronic consequences of the introduction of halide-defects in bulk metal oxides (e.g.  $VO_2$ ). While chlorination of the mixed-valent POV-ethoxide clusters was not possible using  $AlCl_3$ , we have found that the chloride-substituted oxidized derivatives of the Lindqvist vanadium-oxide clusters can be formed using  $TiCl_3(thf)_3$  with  $[V_6O_7(OC_2H_5)]^n$  ( $n = -1, 0$ ) or  $WCl_6$  with  $[V_6O_7(OC_2H_5)]^{1+}$ . Characterization of the chloride-containing products,  $[V_6O_6Cl(OC_2H_5)_{12}]^n$  ( $n = 0, 1+$ ), was accomplished via  $^1H$  NMR spectroscopy, X-ray crystallography, and elemental analysis. Electronic analysis of the redox series of Cl-doped POV-alkoxide clusters via infrared and electronic absorption spectroscopies revealed all redox events are localized to the vanadyl portion of the cluster, with the site differentiated  $V^{III}$ -Cl moiety retaining its reduced oxidation state across a 1.9 V window. These results present new synthetic routes for accessing chloride-doped POV-alkoxide clusters from mixed-valent vanadium oxide precursors.

### Introduction

Anionic defects, in the form of halide ions, are widely observed ‘impurities’ of metal oxides whose assembly typically calls for the use of transition metal halide salt precursors.<sup>1, 2</sup> Notably, these surface-substituted halide ions have been shown to influence the catalytic activity and electronic properties of the material.<sup>3-5</sup> In fact, surface-halogenation of transition metal oxide catalysts with chlorinated gases has been credited as an approach for restoring the activity of “spent” materials.<sup>6-10</sup> Computations and gas-phase reactions of metal oxide moieties have revealed that the cleavage of metal-oxygen bonds via surface halogenation is the first step in the processing of refractory metals (e.g. the conversion of  $V_2O_5$  to  $V^0$ ).<sup>11-15</sup> Likewise, proposed mechanisms for the dehalogenation or oxychlorination of organic substrates with metal oxide catalysts often invoke the substitution of a metal-oxygen bond for a surface-halide ligand.<sup>16-18</sup> Given the significance of halide-functionalized transition metal oxides, interest has emerged in developing an understanding of the electronic influences of surface halogenation of metal ions within these materials.

While gas-phase experiments with molecular “ $V_xO_y$ ” clusters have provided insight into the mechanism of

halogenation at the surface of vanadium oxide,<sup>19-21</sup> the transient nature of the complexes formed makes it difficult to analyse the electronic consequences of surface-defect formation.<sup>22,23</sup> Likewise, direct correlation of electronic structure of surface-halogenated, solid-state, metal oxide systems, to the surface composition of these materials is experimentally challenging. Thus, researchers have turned to the study of discreet, molecular metal oxide clusters as dimensionally reduced models for bulk transition metal oxide materials. Polyoxometalates, in particular, have emerged as promising candidates for these studies, given their elemental composition and delocalized electronic structures.<sup>24-29</sup>

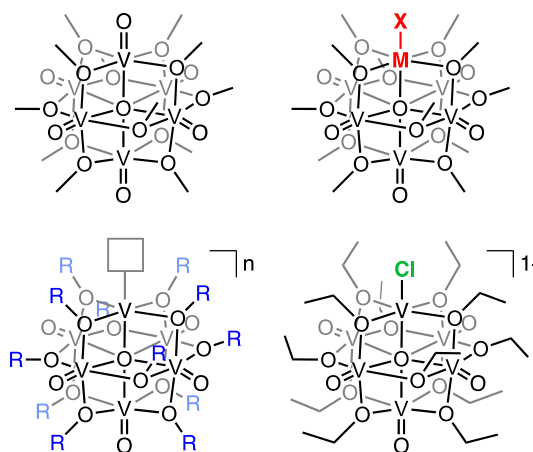


**Figure 1.** Previously reported cation- and anion-doped POV-alkoxide clusters reported by the Matson Laboratory.<sup>30-34, 36-37, 39-40, 44-47</sup>

<sup>a</sup> Department of Chemistry, University of Rochester, Rochester, NY 14627, USA.

<sup>b</sup> E-mail: matson@chem.rochester.edu

Electronic Supplementary Information (ESI) available:  $^1H$  NMR analysis for all complexes, ESI-MS data for complex **6-V<sub>6</sub>O<sub>6</sub>OTf**, crystallographic parameters for complexes **4-V<sub>6</sub>O<sub>6</sub>Cl<sup>0</sup>** (CCDC: 1990064), **5-V<sub>6</sub>O<sub>6</sub>Cl<sup>1+</sup>** (CCDC: 1990062), and **6-V<sub>6</sub>O<sub>6</sub>OTf** (CCDC: 1990063). See DOI: 10.1039/x0xx00000x

Over the past three years, our research group has become interested in the development of metal oxide architectures as solution-phase models for reducible metal oxide surfaces (Figure 1). In particular, we have taken advantage of the unique physicochemical properties of polyoxovanadate-alkoxide (POV-alkoxide) clusters for the formation of discreet, molecular metal oxide systems with surface defects<sup>30, 31</sup> and transition metal dopants.<sup>32-34</sup> POV-alkoxide clusters serve as good models for redox-active, transition metal oxide materials, as they possess Robin and Day Class II delocalized electronic structures, and have surface metal-oxygen bonds available for reactivity.<sup>35-37</sup> However, these molecular systems are distinct from traditional polyoxometalates, as they possess bridging alkoxide ligands that increase their compatibility with organic solvents and provide spectroscopic handles for the analysis of thermally sensitive products (e.g. <sup>1</sup>H NMR). As evidence, we have been able to successfully isolate and characterize unique examples of molecular metal oxide structures bearing oxygen-atom vacancies (defect sites).<sup>30, 31, 38</sup>

Recently, our group reported the first example of site-selective chlorination in POV-alkoxide clusters.<sup>39</sup> Addition of an excess of AlCl<sub>3</sub> to the fully-reduced POV-ethoxide cluster, [V<sup>IV</sup><sub>6</sub>O<sub>7</sub>(OC<sub>2</sub>H<sub>5</sub>)<sub>12</sub>]<sup>2-</sup> resulted in formation of a mono-halogenated species, [V<sup>III</sup>V<sup>IV</sup><sub>4</sub>V<sup>V</sup>O<sub>6</sub>Cl(OC<sub>2</sub>H<sub>5</sub>)<sub>12</sub>]<sup>1-</sup> (**1-V<sub>6</sub>O<sub>6</sub>Cl<sup>1-</sup>**). Our results extended to electrochemical investigations of the electronic consequences of chlorination in the vanadium oxide assembly (Figure 2), which serves as a molecular model for Cl-doped VO<sub>2</sub>. Here, we report the advancement of our chlorination investigations to mixed-valent POV-alkoxide starting materials, namely [V<sup>IV</sup><sub>5</sub>V<sup>V</sup>O<sub>7</sub>(OC<sub>2</sub>H<sub>5</sub>)<sub>12</sub>]<sup>1-</sup> (**2-V<sub>6</sub>O<sub>7</sub><sup>1-</sup>**) and [V<sup>IV</sup><sub>4</sub>V<sup>V</sup><sub>2</sub>O<sub>7</sub>(OC<sub>2</sub>H<sub>5</sub>)<sub>12</sub>] (**3-V<sub>6</sub>O<sub>7</sub><sup>0</sup>**). The results include isolation of the neutral and cationic forms of the monochlorinated POV-alkoxide clusters, [V<sub>6</sub>O<sub>6</sub>Cl(OC<sub>2</sub>H<sub>5</sub>)<sub>12</sub>]<sup>0</sup> (**4-V<sub>6</sub>O<sub>6</sub>Cl<sup>0</sup>**) and [V<sub>6</sub>O<sub>6</sub>Cl(OC<sub>2</sub>H<sub>5</sub>)<sub>12</sub>]<sup>1+</sup> (**5-V<sub>6</sub>O<sub>6</sub>Cl<sup>+</sup>**). Analyses of the isolated series of redoxmers of the Cl-doped POV-alkoxide clusters provides insight into the basis of redox reactions within these materials.

## Results and Discussion

### Syntheses of Cl-doped POVs, [V<sub>6</sub>O<sub>6</sub>Cl(OC<sub>2</sub>H<sub>5</sub>)<sub>12</sub>]<sup>n</sup> (n = 0, +1).

Previous work investigating the halogenation of POV-alkoxide clusters revealed site selective halogenation of a single V<sup>IV</sup>=O

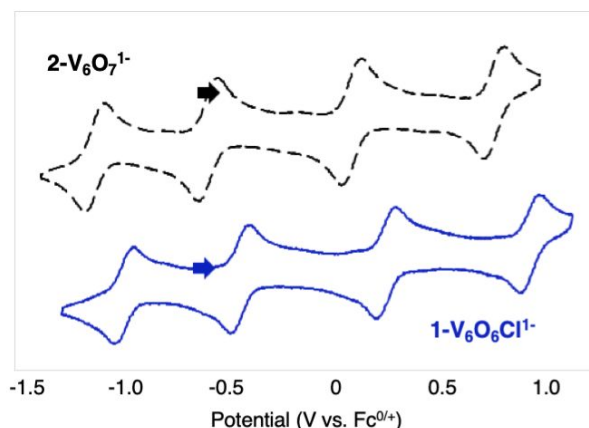
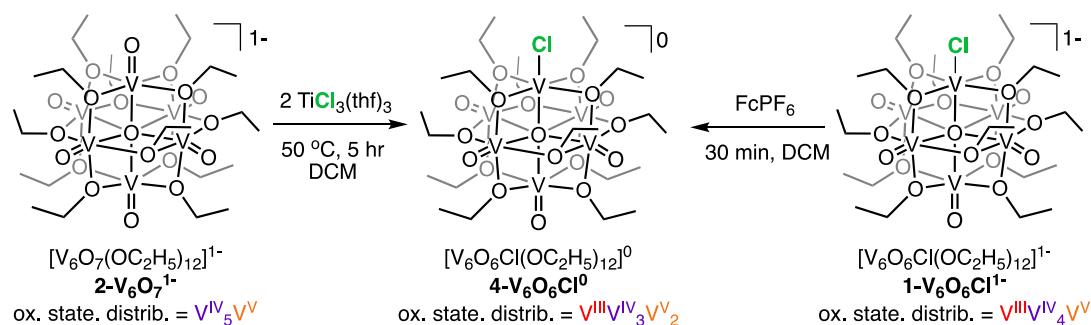


**Figure 2.** Cyclic voltammograms of 1 mM solutions of complexes **1-V<sub>6</sub>O<sub>6</sub>Cl<sup>1-</sup>** (blue) and **2-V<sub>6</sub>O<sub>7</sub><sup>1-</sup>** (black) with 100 mM of [tBu<sub>4</sub>N][PF<sub>6</sub>] in dichloromethane and a scan rate of 500 mV s<sup>-1</sup>.<sup>39</sup>

bond could be achieved by addition of excess AlCl<sub>3</sub> to a solution of either [V<sub>6</sub>O<sub>7</sub>(OC<sub>2</sub>H<sub>5</sub>)<sub>12</sub>]<sup>2-</sup> or [Ti<sub>2</sub>V<sub>4</sub>O<sub>5</sub>(OCH<sub>3</sub>)<sub>14</sub>] in dichloromethane.<sup>40, 39</sup> Notably, both starting materials possess an iso-valent distribution of oxidation states of vanadium centres (i.e. all V<sup>IV</sup>). Attempts to extend the reported reactivity to *mixed-valent* variants of the Lindqvist cluster proved unsuccessful (Figure S1). This result is surprising, particularly given that the cyclic voltammogram (CV) of the previously reported halogenated cluster, **1-V<sub>6</sub>O<sub>6</sub>Cl<sup>1-</sup>**, demonstrates reversible oxidation processes, suggesting stable, oxidized forms of the Cl-doped cluster might be accessible (Figure 2). Intrigued by this finding, we sought to explore new synthetic routes for generating Cl-doped POV-alkoxides of higher oxidation states through direct halogenation of vanadium oxide clusters with mixed-valent electronic structures (complexes **2-V<sub>6</sub>O<sub>7</sub><sup>1-</sup>** and **3-V<sub>6</sub>O<sub>7</sub><sup>0</sup>**).

Initial reactivity studies focused on the mixed-valent POV-alkoxide cluster, **2-V<sub>6</sub>O<sub>7</sub><sup>1-</sup>**, with trimethylsilyl chloride (TMSCl). This reagent has been demonstrated to cleave thermodynamically strong metal-oxygen multiple bonds.<sup>41, 42</sup> In our hands, reactivity of **2-V<sub>6</sub>O<sub>7</sub><sup>1-</sup>** with TMSCl resulted in minimal conversion to a halogenated species, even at elevated temperatures and extended reaction times (Figure S2). We postulate that this is due to the electrophilic nature of the

**Scheme 1.** Synthesis of complex **4-V<sub>6</sub>O<sub>6</sub>Cl<sup>0</sup>**. Reactions cited are unbalanced, given inability to determine the titanium-containing byproduct of these reactions. The stoichiometry indicated represents the reactions that afforded cleanest conversion of the halogenated POV-alkoxide cluster.



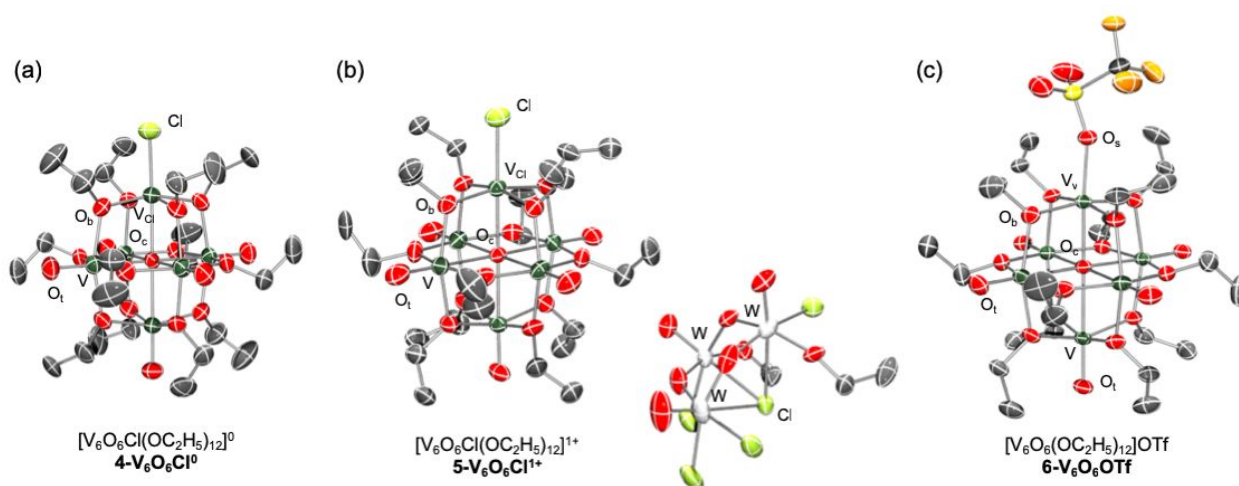


**Figure 3.** Molecular structures of complexes **4- $V_6O_6Cl^0$** , **5- $V_6O_6Cl^{1+}$** , and **6- $V_6O_6OTf$**  shown with 30% probability ellipsoids. Hydrogen atoms, disordered atoms, and solvent molecules have been removed for clarity.

terminal oxide ligands ( $O_t$ ) in POV-alkoxide clusters, a characteristic established through previous reports from our laboratory summarizing the reactivity of  $V=O_t$  moieties in these Lindqvist assemblies.<sup>31, 38</sup> This property inherently makes the exposed oxide ligands less reactive with the trimethylsilyl cation (e.g. TMSCl).

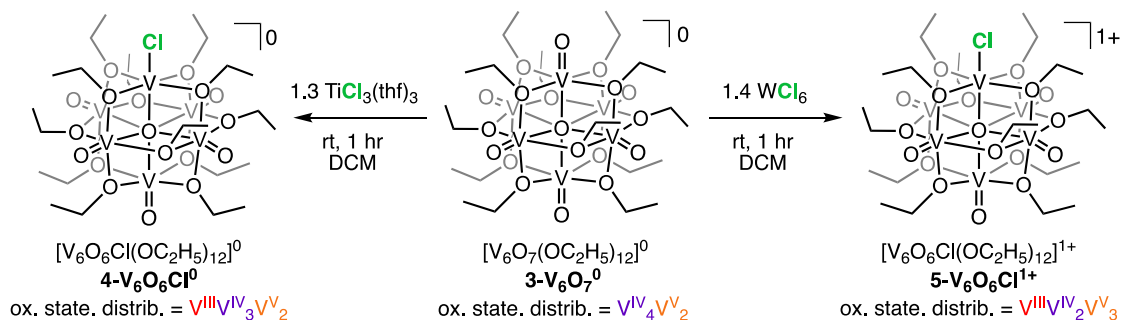
Given the electrophilicity of the terminal oxygen bonds in our POV-alkoxide clusters, we next explored chloride doping with an electron-rich halogenating reagent. We opted to investigate the reactivity of  $TiCl_3(thf)_3$  ( $thf$  = tetrahydrofuran) with complex **2- $V_6O_7^{1-}$** . Addition of two equivalents of  $TiCl_3(thf)_3$  to the mixed-valent POV-alkoxide cluster in dichloromethane afforded a colour change from green to brown (Scheme 1). The reaction was stirred for five hours at 50°C to ensure complete halogenation. Analysis of an aliquot of the crude reaction mixture by  $^1H$  NMR spectroscopy revealed complete consumption of starting material, and conversion to a new product with six distinct paramagnetically shifted and broadened resonances ( $\delta$  = 26.77, 12.52, 5.26, -0.54, -0.92, -20.62 ppm; Figure S3). While the pattern of signals resembles that of complex **1- $V_6O_6Cl^{1-}$**  ( $\delta$  = 25.68, 24.50, 5.73, -0.84, -2.15, -22.67 ppm)<sup>39</sup>, the resonances are

significantly shifted, suggesting possible isolation of a Cl-doped POV-alkoxide cluster in a different oxidation state.

Considering the  $1e^-$  oxidized nature of the POV-alkoxide starting material (**2- $V_6O_7^{1-}$**  vs.  $[V_6O_7(OC_2H_5)_{12}]^{2-}$ ) we posed that the product was likely a Cl-doped vanadium oxide cluster in its neutral charge state (i.e. the one-electron oxidized variant of **1- $V_6O_6Cl^{1-}$** ). To assess the validity of this hypothesis, we sought to independently synthesize the neutral Cl-functionalized POV-alkoxide cluster,  $[V_6O_6Cl(OC_2H_5)_{12}]$  (**4- $V_6O_6Cl^0$** ), via oxidation of complex **1- $V_6O_6Cl^{1-}$**  (Scheme 1). Analysis of the reaction mixture of one equivalent of ferrocenium hexafluorophosphate ( $FcPF_6$ ;  $E_{1/2}$  = 0.00 V vs.  $Fc^{0/+}$ )<sup>43</sup> and **1- $V_6O_6Cl^{1-}$**  revealed formation of ferrocene and a new paramagnetic product, as confirmed by  $^1H$  NMR spectroscopy ( $\delta$  = 26.53, 12.48, 5.30, -0.54, -0.92, -20.47 ppm; Figure S4). These resonances match those described above for the product of the reaction of complex **2- $V_6O_7^{1-}$**  and  $TiCl_3(thf)_3$ .

To unambiguously determine the molecular structure of the product of the aforementioned reactions, crystals suitable for X-ray diffraction were grown from slow diffusion of pentane into a concentrated solution of complex **4- $V_6O_6Cl^0$**  in tetrahydrofuran (Figure 3, Table S1). While single crystal X-ray data confirmed connectivity and composition of **4- $V_6O_6Cl^0$** ,

**Scheme 2.** Reactivity of **3- $V_6O_7^0$**  with metal chloride salts: Syntheses of complexes **4- $V_6O_6Cl^0$**  and **5- $V_6O_6Cl^{1+}$** . Reactions cited are unbalanced, given inability to determine the titanium- and tungsten-containing byproducts of these reactions. The stoichiometry indicated represents the reactions that afforded cleanest conversion of the halogenated POV-alkoxide cluster.

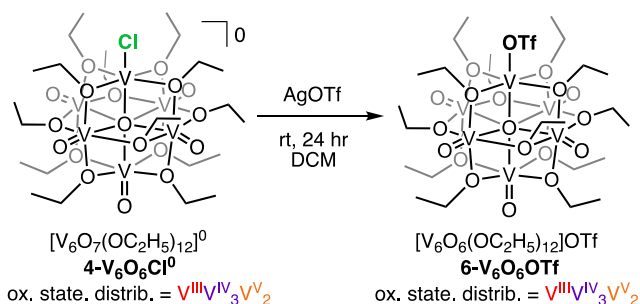


rigorous analysis of bond metrics within the Lindqvist assembly was not possible due to disorder within the unit cell. The asymmetric unit contains one-fourth of a cluster located at a crystallographic  $2/m$  position that coincides with the central oxygen atom. The two unique terminal ligand sites were modelled as disorders of O and Cl, fixed in a summed ratio of 1.66667:0.33333, which was the ratio established from known synthetic and independent spectroscopic means. As a test, when the occupancies at the two sites were allowed to refine independently, the ratios and  $R1$  (strong data) remained essentially the same. For the two unique terminal ligand site disorders, the V-O and V-Cl bond lengths were restrained to be similar, respectively. More minor disorder was noted in the ethoxide ligands, which were best modelled over two positions (see supporting information and crystallographic information file for more details). Analogous bond lengths and angles for the disordered ethoxide ligands were restrained to be similar.

To assess the generality of  $\text{TiCl}_3(\text{thf})_3$  as a reagent for halogenating the surface of POV-alkoxide clusters, we added one equivalent to the fully reduced vanadium oxide assembly,  $[\text{V}_6\text{O}_7(\text{OC}_2\text{H}_5)_{12}]^{2-}$ . In accordance with results reported previously by our group,<sup>39</sup> conversion of the fully oxygenated POV-alkoxide cluster to the mono-halogenated species,  $\mathbf{1-V}_6\text{O}_6\text{Cl}^-$  was confirmed by  $^1\text{H}$  NMR spectroscopy (Figure S5; yield determined by  $^1\text{H}$  NMR spectroscopy). This result suggests that  $\text{TiCl}_3(\text{thf})_3$  is an adequate reagent for the selective halogenation of these Lindqvist-type vanadium oxide assemblies across multiple oxidation states.

Following the observation of a redox-neutral halogenation reaction upon addition of  $\text{TiCl}_3(\text{thf})_3$  to complexes  $\mathbf{2-V}_6\text{O}_7^{1-}$  and  $[\text{V}_6\text{O}_7(\text{OC}_2\text{H}_5)_{12}]^{2-}$ , we next attempted the synthesis of the cationic form of a Cl-doped vanadium oxide assembly, namely  $[\text{V}_6\text{O}_6\text{Cl}(\text{OC}_2\text{H}_5)_{12}]^+$  ( $\mathbf{5-V}_6\text{O}_6\text{Cl}^+$ ) via halogenation of complex  $\mathbf{3-V}_6\text{O}_7^0$  (Scheme 2). Addition of an excess of  $\text{TiCl}_3(\text{thf})_3$  to a solution of  $\mathbf{3-V}_6\text{O}_7^0$  in dichloromethane again afforded a colour change from green to brown over the course of one hour. To our surprise, inspection of the reaction mixture following work-up by  $^1\text{H}$  NMR spectroscopy suggested formation of complex  $\mathbf{4-V}_6\text{O}_6\text{Cl}^0$  as the major product, as opposed to the expected cationic form of the Cl-doped cluster (Figure S6).

We reasoned isolation of the reduced form of the Cl-doped POV-alkoxide cluster was likely a result of intermolecular electron transfer from the  $\text{Ti}^{\text{III}}$  halogenating reagent to the more-oxidized POV-alkoxide precursor. To assess the validity of this hypothesis, a CV of  $\text{TiCl}_3(\text{thf})_3$  was collected in dichloromethane (Figure S7). A poorly-resolved, quasi-reversible redox event was noted in the voltammogram with an  $E_{1/2}$  value of  $-0.52$  V (vs.  $\text{Fc}^{0/+}$ ). This potential is insufficient to convert the fully-oxygenated POV-alkoxide precursor,  $\mathbf{3-V}_6\text{O}_7^0$ , to its more reduced form,  $\mathbf{2-V}_6\text{O}_7^{1-}$ , prior to surface halogenation ( $E_{1/2} [\text{V}_6\text{O}_7(\text{OC}_2\text{H}_5)_{12}]^{1/0} = -0.62$  V vs.  $\text{Fc}^{0/+}$ ).<sup>39</sup> However, halogenation of the cluster surface affords a shift in the redox potential of the resultant Cl-doped POV-alkoxide cluster,  $\mathbf{5-V}_6\text{O}_6\text{Cl}^+$ , by approximately  $0.7$  V ( $E_{1/2} [\text{V}_6\text{O}_6\text{Cl}(\text{OC}_2\text{H}_5)_{12}]^{0/1+} = +0.23$  V vs.  $\text{Fc}^{0/+}$ ), consistent with a change in surface charge density of the metal oxide assembly.

Scheme 3. Synthesis of  $\mathbf{6-V}_6\text{O}_6\text{OTf}$ .

This change in redox potential renders the Cl-doped variant easily reduced by  $\text{TiCl}_3(\text{thf})_3$ . Thus, we can conclude, mechanistically, that ligand substitution at the cluster surface must occur prior to the electron transfer process that results in isolation of complex  $\mathbf{4-V}_6\text{O}_6\text{Cl}^0$ .

To independently isolate the oxidized form of the Cl-doped POV-alkoxide cluster, suggested to form transiently during the halogenation of  $\mathbf{3-V}_6\text{O}_7^0$  with  $\text{TiCl}_3(\text{thf})_3$ , we turned to cluster oxidation. Fortuitously, the oxidation potential of complex  $\mathbf{4-V}_6\text{O}_6\text{Cl}^0$  ( $E_{1/2} [\text{V}_6\text{O}_6\text{Cl}(\text{OC}_2\text{H}_5)_{12}]^{0/1+} = +0.23$  V vs.  $\text{Fc}^{0/+}$ ) is easily accessed by a variety of oxidizing reagents.<sup>43</sup> We opted to attempt cluster oxidation using  $\text{AgOTf}$  in dichloromethane, given its ideal redox potential for selective oxidation to the desired monocationic species ( $E_{1/2} \text{Ag}^{0/+} = 0.65$  V vs.  $\text{Fc}^{0/+}$ ),<sup>43</sup> as well as the weakly-coordinating properties of the trifluoromethylsulfonate anion. Addition of one equivalent of  $\text{AgOTf}$  to complex  $\mathbf{4-V}_6\text{O}_6\text{Cl}^0$  resulted in a cloudy, dark, green-brown solution. Following work-up, analysis of the product by  $^1\text{H}$  NMR spectroscopy revealed a new set of paramagnetically broadened and shifted resonances ( $\delta = 26.57, 12.49, 5.85, -0.78, -23.09$  ppm; Figure S8), consistent with the anticipated oxidation of the Cl-doped POV-alkoxide cluster. However, further characterization of the product by electrospray ionization mass spectrometry (ESI-MS), indicated an atomic mass consistent with the triflate-bound POV-alkoxide cluster,  $[\text{V}_6\text{O}_6(\text{OC}_2\text{H}_5)_{12}]\text{OTf}$  (ESI-MS (-)ve mode,  $m/z = 1091$ ; Figure S9). This result was consistent with elemental analysis performed on the sample.

Given these results, we can conclude that a ligand exchange (salt metathesis) reaction occurs upon addition of  $\text{AgOTf}$  to complex  $\mathbf{4-V}_6\text{O}_6\text{Cl}^0$ , substituting the terminal chloride ligand for a weakly-coordinating trifluoromethylsulfonate entity (Scheme 3). Absolute support for product formulation was obtained via single crystal X-ray diffraction. Refinement of structural data collected on dark green crystals grown from slow diffusion of diethyl ether into a concentrated solution of  $\mathbf{6-V}_6\text{O}_6\text{OTf}$  revealed a Lindqvist ion with a single terminal oxido moiety substituted by a trifluoromethylsulfonate ligand (Figure 3, Table S1). The molecular structure resembles closely that reported for its methoxide-ligand congener,  $[\text{V}_6\text{O}_6(\text{OCH}_3)_{12}]\text{OTf}$ , reported previously by our laboratory.<sup>31</sup>

We hypothesized that isolation of the desired cationic form of the Cl-doped POV-alkoxide cluster,  $5\text{-V}_6\text{O}_6\text{Cl}^{1+}$ , might be possible through the use of a more oxidizing metal halide precursor. Thus, we opted to explore the reactivity of  $\text{WCl}_6$  ( $E_{1/2} = 1.1$  V vs.  $\text{Fc}^{0/+}$ )<sup>43</sup> with  $3\text{-V}_6\text{O}_7^0$ , posing that the combination of oxophilic and oxidizing properties of the high-valent tungsten ion would facilitate formation of the desired monocationic, halogenated species. The addition of  $\text{WCl}_6$  to complex  $3\text{-V}_6\text{O}_7^0$  resulted in an immediate reaction, yielding a dark brown precipitate and an orange-brown solution (Scheme 2).  $^1\text{H}$  NMR analysis of the filtrate revealed formation of a set of paramagnetically shifted and broadened resonances ( $\delta = 16.49, 10.19, 8.48, 0.77, 0.20, -0.55, -21.85$  ppm; Figure S10, distinct from those observed for complexes  $1\text{-V}_6\text{O}_6\text{Cl}^{1-}$ ,  $4\text{-V}_6\text{O}_6\text{Cl}^0$ , and  $6\text{-V}_6\text{O}_6\text{OTf}$ .

Confirmation of formation of the desired cationic form of the Cl-doped POV-alkoxide cluster was obtained from crystallographic analysis. Single crystals of complex  $5\text{-V}_6\text{O}_6\text{Cl}^{1+}$ , suitable for X-ray diffraction, were grown by slow diffusion of pentane into a concentrated solution of the cluster in dichloromethane (Figure 3, Table S1). Refinement of the data revealed a chloride-functionalized Lindqvist POV-alkoxide, with a tungsten-derived counter ion,  $[\text{W}_3\text{O}_6\text{Cl}_5(\text{OEt})_2]^{1-}$ . The presence of this tungsten-containing anion provides insight into the fate of the metal chloride halogenating reagent used in this reaction; indeed, oxygen atom transfer from the POV-alkoxide to a tungsten ion resultant from the chlorination of the cluster surface must occur, as indicated by the presence of new W-O linkages not present in the starting material.

While complex  $5\text{-V}_6\text{O}_6\text{Cl}^{1+}$  crystallizes with each vanadium centre of the Lindqvist cluster in a unique crystallographic position within the unit cell, the poor quality of the structural data renders bond-metric analysis of this sample unreliable (see supporting information and crystallographic information file for more information). Despite exhaustive attempts, we were unable to collect crystals of better quality for analysis. However, the connectivity of the sample is unambiguous, providing supporting evidence for the formation of the monocationic Cl-doped POV-alkoxide cluster.

#### Spectroscopic Analysis of Cl-doped POV-alkoxide Clusters.

To elucidate the identity of vanadium ions involved in oxidation of the Cl-doped POV-alkoxide clusters, we performed spectroscopic analyses on complexes  $4\text{-V}_6\text{O}_6\text{Cl}^0$  and  $5\text{-V}_6\text{O}_6\text{Cl}^{1+}$ . The evenly-spaced electrochemical events observed in the cyclic voltammogram of the Cl-doped POV-alkoxide are consistent with other Lindqvist vanadium-oxide clusters reported by our laboratory, all of which have their redox chemistry localized to vanadyl ions of the Lindqvist core (Figure 2).<sup>44-47</sup> Given the previously reported oxidation state distribution of the monoanionic form of the cluster,  $1\text{-V}_6\text{O}_6\text{Cl}^{1-}$  ( $[\text{V}^{\text{III}}\text{V}_4\text{V}^{\text{V}}]$ ), we hypothesized that the electrochemistry of the surface-halogenated POV-ethoxide cluster would be localized to the vanadyl assembly, with retention of the  $\text{V}^{\text{III}}\text{-Cl}$  entity across all charge states.

Our group<sup>30, 31, 33, 38, 44, 46, 47</sup> and others<sup>36, 37</sup> have shown that infrared and electronic absorption spectroscopies are powerful

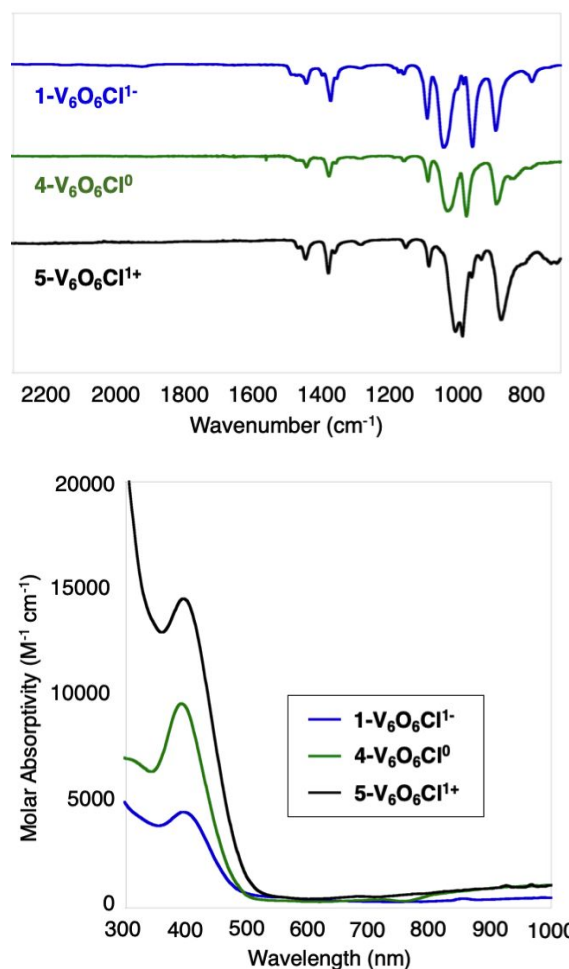


Figure 4. Infrared (top) and electronic absorption spectra (bottom) of  $1\text{-V}_6\text{O}_6\text{Cl}^{1-}$  (blue),  $4\text{-V}_6\text{O}_6\text{Cl}^0$  (green), and  $5\text{-V}_6\text{O}_6\text{Cl}^{1+}$  (black). Absorption spectra collected in dichloromethane at 21 °C.

tools for understanding the changes in the electronic structure of POV-alkoxide clusters across a series of oxidation states. Thus, with the chloride-functionalized POV-alkoxide clusters in hand, we sought to elucidate the origin of the rich redox chemistry of these halogenated systems. The IR spectra of complexes  $1\text{-V}_6\text{O}_6\text{Cl}^{1-}$ ,  $4\text{-V}_6\text{O}_6\text{Cl}^0$ , and  $5\text{-V}_6\text{O}_6\text{Cl}^{1+}$  are shown in Figure 4, with values summarized in Table 1. Upon oxidation, the transition assigned to the  $\nu(\text{V}=\text{O}_t)$  stretching mode shifts toward higher energies ( $1\text{-V}_6\text{O}_6\text{Cl}^{1-}$ : 956  $\text{cm}^{-1}$ ;  $4\text{-V}_6\text{O}_6\text{Cl}^0$ : 974  $\text{cm}^{-1}$ ;  $5\text{-V}_6\text{O}_6\text{Cl}^{1+}$ : 986  $\text{cm}^{-1}$ ), consistent with the oxidation of  $\text{V}=\text{O}$  moieties across the Lindqvist core. This change in  $\nu(\text{V}=\text{O}_t)$  is accompanied by a shift in the  $\nu(\text{O}-\text{C}_2\text{H}_5)$  band toward lower energies, ( $1\text{-V}_6\text{O}_6\text{Cl}^{1-}$ : 1040  $\text{cm}^{-1}$ ;  $4\text{-V}_6\text{O}_6\text{Cl}^0$ : 1030  $\text{cm}^{-1}$ ;  $5\text{-V}_6\text{O}_6\text{Cl}^{1+}$ : 1006  $\text{cm}^{-1}$ ). The change in the energy difference between these two diagnostic bands ( $\Delta E_b$ ) correlates to a depletion in charge density of the vanadyl-containing portion of the POV-alkoxide cluster (values summarized in Table 1). Indeed, we have observed similar magnitudes in  $\Delta E_b$  in our work with iron-functionalized POV-alkoxide clusters, where the redox chemistry has been assigned to oxidation/reduction of the vanadyl moieties of the heterometal-functionalized POV-alkoxide cluster.<sup>44, 45</sup>

**Table 1.** Tabulated values for infrared and electronic absorption spectroscopic data for complexes **1-V<sub>6</sub>O<sub>6</sub>Cl<sup>-</sup>**, **4-V<sub>6</sub>O<sub>6</sub>Cl<sup>0</sup>**, **5-V<sub>6</sub>O<sub>6</sub>Cl<sup>1+</sup>**, [V<sub>6</sub>O<sub>6</sub>(OC<sub>2</sub>H<sub>5</sub>)<sub>12</sub>(MeCN)]<sup>0</sup>, and **6-V<sub>6</sub>O<sub>6</sub>OTf**. Predicted oxidation state distributions for each cluster listed to aid in data interpretation.

Compound	Ox. State Distrib.	Infrared Spectroscopy			Electronic Absorption Spectroscopy	
		$\nu(\text{O}_b\text{-R})$	$\nu(\text{V}=\text{O}_i)$	$\Delta E_b$	Wavelengths and molar absorptivity values of IVCT bands	
<b>1-V<sub>6</sub>O<sub>6</sub>Cl<sup>-</sup></b> <sup>a</sup>	V <sup>III</sup> V <sup>IV</sup> <sub>4</sub> V <sup>V</sup>	1040 cm <sup>-1</sup>	956 cm <sup>-1</sup>	84 cm <sup>-1</sup>	398 nm ( $\epsilon = 4495 \text{ M}^{-1} \text{ cm}^{-1}$ )	1000 nm ( $\epsilon = 478 \text{ M}^{-1} \text{ cm}^{-1}$ )
<b>4-V<sub>6</sub>O<sub>6</sub>Cl<sup>0</sup></b>	V <sup>III</sup> V <sup>IV</sup> <sub>3</sub> V <sup>V</sup> <sub>2</sub>	1030 cm <sup>-1</sup>	974 cm <sup>-1</sup>	56 cm <sup>-1</sup>	394 nm ( $\epsilon = 9599 \text{ M}^{-1} \text{ cm}^{-1}$ )	1000 nm ( $\epsilon = 1047 \text{ M}^{-1} \text{ cm}^{-1}$ )
<b>5-V<sub>6</sub>O<sub>6</sub>Cl<sup>1+</sup></b>	V <sup>III</sup> V <sup>IV</sup> <sub>2</sub> V <sup>V</sup> <sub>3</sub>	1006 cm <sup>-1</sup>	986 cm <sup>-1</sup>	20 cm <sup>-1</sup>	395 nm ( $\epsilon = 16700 \text{ M}^{-1} \text{ cm}^{-1}$ )	1000 nm ( $\epsilon = 1238 \text{ M}^{-1} \text{ cm}^{-1}$ )
[V <sub>6</sub> O <sub>6</sub> (OC <sub>2</sub> H <sub>5</sub> ) <sub>12</sub> (MeCN)] <sup>0</sup> <sup>b</sup>	V <sup>III</sup> V <sup>IV</sup> <sub>4</sub> V <sup>V</sup>	1041 cm <sup>-1</sup>	964 cm <sup>-1</sup>	77 cm <sup>-1</sup>	394 nm ( $\epsilon = 2793 \text{ M}^{-1} \text{ cm}^{-1}$ )	1000 nm ( $\epsilon = 417 \text{ M}^{-1} \text{ cm}^{-1}$ )
<b>6-V<sub>6</sub>O<sub>6</sub>OTf</b>	V <sup>III</sup> V <sup>IV</sup> <sub>3</sub> V <sup>V</sup> <sub>2</sub>	1028 cm <sup>-1</sup>	980 cm <sup>-1</sup>	48 cm <sup>-1</sup>	392 nm ( $\epsilon = 11393 \text{ M}^{-1} \text{ cm}^{-1}$ )	1000 nm ( $\epsilon = 1409 \text{ M}^{-1} \text{ cm}^{-1}$ )

<sup>a</sup> Infrared and electronic absorption spectroscopic data taken from previously reported data for complex **1-V<sub>6</sub>O<sub>6</sub>Cl<sup>-</sup>**<sup>39</sup>; <sup>b</sup> Infrared and electronic absorption spectroscopic data taken from previously reported data for [V<sub>6</sub>O<sub>6</sub>(OC<sub>2</sub>H<sub>5</sub>)<sub>12</sub>(MeCN)]<sup>0</sup><sup>38</sup>

Assignment of the location of oxidation was further confirmed by electronic absorption spectroscopy (Figure 4, Table 1). As the cluster is sequentially oxidized from **1-V<sub>6</sub>O<sub>6</sub>Cl<sup>-</sup>** to **5-V<sub>6</sub>O<sub>6</sub>Cl<sup>1+</sup>**, an increase in the molar absorptivities of the intervalence charge transfer (IVCT) bands of the mixed-valent POV-alkoxide cluster is observed. The higher energy feature corresponds to the  $d_{xy}(\text{V}^{\text{IV}}) \rightarrow d_{x^2-y^2}(\text{V}^{\text{V}})$  intervalence charge transfer (IVCT), while the lower energy is assigned to a  $d_{xy}(\text{V}^{\text{IV}}) \rightarrow d_{xy}(\text{V}^{\text{IV}})$  IVCT event.<sup>36-37</sup> The increase in intensity of the IVCT bands observed at 394 nm and 1000 nm upon formation of complex **4-V<sub>6</sub>O<sub>6</sub>Cl<sup>0</sup>** is consistent with a one-electron oxidation over the Class II delocalized vanadyl-sites of the POV-alkoxide framework.<sup>35</sup> The greater number of d<sup>0</sup> centres within the Lindqvist cluster increases the probability of the occurrence of a charge transfer event for the system, correlating to a larger molar absorptivity for these absorption events. Upon further oxidation of the cluster to generate complex **5-V<sub>6</sub>O<sub>6</sub>Cl<sup>1+</sup>**, a similar increase in intensity is observed in the high-energy IVCT band (~ 390 nm), while the molar absorptivity of the transition at lower energy (1000 nm) remains similar in magnitude to that of complex **4-V<sub>6</sub>O<sub>6</sub>Cl<sup>0</sup>** (Table 1). It is helpful at this point to consider that the larger molar absorptivity values of the high-energy band is due to overlap with a ligand-to-metal charge-transfer event, in which lone pairs of electron density of the terminal oxide ligands are donated to the electron deficient vanadium ions.<sup>36, 37</sup> This electronic transition is amplified as oxidation of the POV-alkoxide cluster occurs, such that electrons are more efficiently transferred from the oxide-ligands as the electron density of the cluster core is depleted.

With these results, we can assign the oxidation state distributions of vanadium centres within the series of chloride-functionalized POV-alkoxide clusters. As described above, complex **1-V<sub>6</sub>O<sub>6</sub>Cl<sup>-</sup>** possesses an oxidation state distribution of V<sup>III</sup>V<sup>IV</sup><sub>4</sub>V<sup>V</sup>, providing a starting point for our analysis. Given that each oxidation event, as supported by IR and electronic absorption spectroscopies, occurs across the five V=O moieties of the Lindqvist core, the oxidation state distributions of vanadium ions in complexes **4-V<sub>6</sub>O<sub>6</sub>Cl<sup>0</sup>** and **5-V<sub>6</sub>O<sub>6</sub>Cl<sup>1+</sup>** can be described as V<sup>III</sup>V<sup>IV</sup><sub>3</sub>V<sup>V</sup><sub>2</sub> and V<sup>III</sup>V<sup>IV</sup><sub>2</sub>V<sup>V</sup><sub>3</sub>, respectively.

The isolation of redox chemistry to vanadate moieties within the Cl-doped POV-alkoxide cluster is not wholly

surprising, given our previous results demonstrating similar localized electrochemical properties in other site-differentiated POV-alkoxide clusters.<sup>32, 44, 45</sup> However, taken as models for Cl-doped vanadium oxides, these results present interesting perspectives on the possible role of anionic dopants in modulating the electronic properties of bulk metal oxide systems. Notably, the introduction of the chloride ligand sufficiently decouples the new, low-valent V<sup>III</sup> centre from remaining metals in the metal oxide framework, introducing a defect site into the assembly. Across all charge states of the Cl-doped POV-alkoxide cluster (complexes **1-V<sub>6</sub>O<sub>6</sub>Cl<sup>-</sup>**, **4-V<sub>6</sub>O<sub>6</sub>Cl<sup>0</sup>**, and **5-V<sub>6</sub>O<sub>6</sub>Cl<sup>1+</sup>**), the reduced V<sup>III</sup> ion retains its oxidation state. This result provides concrete evidence that the dopant does not change the *nature* of redox chemistry in the cluster; all reversible redox events remain associated with V<sup>IV</sup>/V<sup>V</sup> couples of vanadyl ions.

The introduction of a chloride ligand at a single vanadium centre results in significant shifts in redox potentials of these electrochemical events, as described previously by our research team (Figure 2).<sup>39</sup> In that work, we summarize that the observed shifts are consistent with the proposed effects of halogenation of VO<sub>2</sub>, supporting the role of defect engineering in the tuning of the band edges of metal oxides. In analogy to the predicted band edge diagrams for halide-doped VO<sub>2</sub>,<sup>48</sup> we do not observe evidence for the formation of new redox events that could be associated with mid-gap states in the bulk solid. This result is notable, given that the introduction of defect sites in semiconducting metal oxides is associated with the formation of these mid-gap states.<sup>49-53</sup> The manipulation of the electronic structure of the material rests solely on the modulation of the energies of vanadium- and oxygen-derived orbitals in both the material, VO<sub>2</sub>, as well as in our model system.

## Conclusions

In this work, we have expanded upon our previous report describing a synthetic route for forming a Cl-doped POV-alkoxide cluster. In our original study, addition of AlCl<sub>3</sub> to the fully reduced cluster, [V<sub>6</sub>O<sub>7</sub>(OC<sub>2</sub>H<sub>5</sub>)<sub>12</sub>]<sup>2-</sup>, resulted in V=O bond cleavage, and formation of a unique V<sup>III</sup>-Cl moiety within the

hexavanadate assembly.<sup>39</sup> While  $\text{AlCl}_3$  proved to efficiently halogenate the surface of the dianionic, isovalent ( $[\text{V}^{\text{IV}}_6]$ ) POV-ethoxide cluster, this reagent was unreactive with mixed-valent (i.e. more-oxidized) forms of the Lindqvist vanadium-oxide assembly. Here, we demonstrate two new synthetic approaches for the surface halogenation of mixed-valent vanadium oxide clusters. Addition of metal chloride salts (e.g.  $\text{TiCl}_3(\text{thf})_3$ ,  $\text{WCl}_6$ ) to the monoanionic and neutral POV-ethoxide complexes,  $\mathbf{2-V_6O_7^{1-}}$  or  $\mathbf{3-V_6O_7^0}$ , results in ligand substitution at the surface of the Lindqvist core. In both cases, isolation of mono-chlorinated, mixed-valent POV-alkoxide clusters,  $\mathbf{4-V_6O_6Cl^0}$  and  $\mathbf{5-V_6O_6Cl^{1+}}$ , proved possible.

With the isolation of a series of redoxmers of the Cl-doped POV-alkoxide clusters in hand, analysis of the electronic structures (oxidation state distribution of metal ions) was performed. Characterization of  $\mathbf{1-V_6O_6Cl^{1-}}$ ,  $\mathbf{4-V_6O_6Cl^0}$ , and  $\mathbf{5-V_6O_6Cl^{1+}}$  via infrared and electronic absorption spectroscopies reveals all redox chemistry of the cluster is localized to the vanadium-oxide core (as opposed to the site-differentiated  $\text{V}^{\text{III}}$ -Cl moiety). This mirrors the calculated electronic consequences (e.g. shifts in band edges) of halogenation of bulk  $\text{VO}_2$ .

## Experimental.

**General Considerations.** All manipulations, unless otherwise noted, were carried out in the absence of water and oxygen in a UniLab MBraun inert atmosphere glovebox under a dinitrogen atmosphere. Glassware was oven dried for a minimum of 4 hrs and cooled in an evacuated antechamber prior to use in the drybox. Unless otherwise noted, solvents were dried and deoxygenated on a Glass Contour System (Pure Process Technology, LLC) and stored over activated 3 Å molecular sieves purchased from Fisher Scientific.  $\text{TiCl}_3(\text{thf})_3$ <sup>54</sup>,  $[\text{nBu}_4\text{N}][\text{V}_6\text{O}_6\text{Cl}(\text{OC}_2\text{H}_5)_{12}]$  ( $\mathbf{1-V_6O_6Cl^{1-}}$ )<sup>39</sup>,  $[\text{nBu}_4\text{N}][\text{V}_6\text{O}_7(\text{OC}_2\text{H}_5)_{12}]$  ( $\mathbf{2-V_6O_7^{1-}}$ )<sup>46</sup>,  $[\text{nBu}_4\text{N}]_2[\text{V}_6\text{O}_7(\text{OC}_2\text{H}_5)_{12}]$ <sup>46</sup> and  $[\text{V}_6\text{O}_7(\text{OC}_2\text{H}_5)_{12}]^0$  ( $\mathbf{3-V_6O_7^0}$ )<sup>36</sup> were prepared as previously reported.  $\text{AlCl}_3$ ,  $\text{TMSCl}$ ,  $\text{FcPF}_6$  and  $\text{WCl}_6$  were purchased from Sigma Aldrich and used as received.

<sup>1</sup>H NMR spectra were recorded at 400 MHz on Bruker DPX-400 MHz spectrometers locked on the signal of deuterated solvents. All chemical shifts were reported relative to the peak of residual <sup>1</sup>H signal in deuterated solvents.  $\text{CDCl}_3$  and  $\text{CD}_2\text{Cl}_2$  were purchased from Cambridge Isotope Laboratories, degassed by three freeze-pump-thaw cycles, and stored over activated 3 Å molecular sieves. Infrared (FT-IR, ATR) spectra of complexes were recorded on a Shimadzu IRAffinity-1 Fourier Transform Infrared Spectrophotometer and are reported in wavenumbers ( $\text{cm}^{-1}$ ). Electronic absorption measurements were recorded at room temperature in anhydrous dichloromethane in a sealed 1 cm quartz cuvette with an Agilent Cary 60 UV-Vis spectrophotometer. Mass spectrometry analyses were performed on an Advion Expression<sup>1</sup> Compact Mass Spectrometer equipped with an electrospray probe and an ion-trap mass analyser. Direct injection analysis was employed in all cases with a sample solution in acetonitrile. Single crystals were mounted on the tip of a thin glass optical fiber (goniometer head) and mounted on a Bruker SMART

APEX II CCD platform diffractometer for a data collection at 100.0(5) K. The structures were solved using SHELXT-2014/5<sup>55</sup> and refined using SHELXL-2014/7<sup>56</sup>. Elemental analyses were performed on by Midwest Microlabs in Indianapolis, Indiana.

### Synthesis of $\text{V}_6\text{O}_6\text{Cl}(\text{OC}_2\text{H}_5)_{12}$ ( $\mathbf{4-V_6O_6Cl^0}$ )

**Method A.** A 20 mL scintillation vial was charged with  $\mathbf{2-V_6O_7^{1-}}$  (0.044 g, 0.037 mmol) and  $\text{TiCl}_3(\text{thf})_3$  (0.027 g, 0.072 mmol). Dichloromethane (6 mL) was added, and the reaction was stirred at 50°C for 5 hours. The dark green mixture was filtered, and volatiles were removed under reduced pressure. The solid was stirred in 6 mL of diethyl ether for 2 hours, then the solid was washed with diethyl ether until it ran clear. Volatiles were removed under reduced pressure to obtain  $\mathbf{4-V_6O_6Cl^0}$  as a yellow-brown solid (23%, yield determined by <sup>1</sup>H NMR spectroscopy, see supporting information for details). <sup>1</sup>H NMR (400 MHz,  $\text{CDCl}_3$ )  $\delta$  = 26.53 (fwhh = 260 Hz), 12.48 (fwhh = 240 Hz), 5.30 (fwhh = 24 Hz), -0.54 (fwhh = 120 Hz), -0.92 (fwhh = 120 Hz), -20.47 (fwhh = 500 Hz) ppm.

**Method B.** A 20 mL scintillation vial was charged with complex  $\mathbf{1-V_6O_6Cl^{1-}}$  (0.053 g, 0.0542 mmol) and 3 mL of dichloromethane. In a separate vial, ferrocenium hexafluorophosphate ( $\text{FcPF}_6$ ; 0.025 g, 0.075 mmol) was dissolved in 3 mL of dichloromethane. The  $\text{FcPF}_6$  solution was added dropwise to  $\mathbf{1-V_6O_6Cl^{1-}}$  with vigorous stirring. An additional 2 mL of dichloromethane was used to ensure complete transfer of  $\text{FcPF}_6$  into the reaction mixture. After 30 minutes, volatiles were removed under reduced pressure, leaving a dark brown residue. The solid was washed with pentane (4 mL x 5) until the filtrate ran clear. The remaining solid was then extracted with tetrahydrofuran, filtered, and the volatiles were removed under reduced pressure. The final product,  $\mathbf{4-V_6O_6Cl^0}$ , was isolated as a yellow-brown solid in good yield (0.053 g, 0.054 mmol, 75 %). Crystals suitable for X-ray crystallography were grown by the slow diffusion of pentane into a concentrated solution of tetrahydrofuran. <sup>1</sup>H NMR analysis of this sample matched that described for complex  $\mathbf{4-V_6O_6Cl^0}$  described in Method A. FT-IR (ATR,  $\text{cm}^{-1}$ ): 1030 ( $\text{O}_b\text{-C}_2\text{H}_5$ ), 974 ( $\text{V=O}_i$ ). UV-Vis ( $\text{CH}_2\text{Cl}_2$ ): 394 nm, ( $\epsilon$  = 9599  $\text{M}^{-1}\text{cm}^{-1}$ ), 1000 nm ( $\epsilon$  = 1047  $\text{M}^{-1}\text{cm}^{-1}$ ). Elemental analysis for  $\text{C}_{24}\text{H}_{60}\text{O}_{18}\text{V}_6\text{Cl}$  (MW = 977.48 g/mol) Calcd (%): C, 29.46; H, 6.19. Found (%): C, 29.71; H, 6.09.

### Synthesis of $[\text{nBu}_4\text{N}][\text{V}_6\text{O}_6\text{Cl}(\text{OC}_2\text{H}_5)_{12}]$ ( $\mathbf{1-V_6O_6Cl^{1-}}$ ) via chlorination of $[\text{V}_6\text{O}_7(\text{OC}_2\text{H}_5)_{12}]^{2-}$ with $\text{TiCl}_3(\text{thf})_3$

A 20 mL scintillation vial was charged with  $[\text{nBu}_4\text{N}]_2[\text{V}_6\text{O}_7(\text{OC}_2\text{H}_5)_{12}]$  (0.040 g, 0.028 mmol) and  $\text{TiCl}_3(\text{thf})_3$  (0.009 g, 0.025 mmol). Tetrahydrofuran (6 mL) was added, and the reaction was stirred at 70 °C for 1 hour. The resultant orange-brown solution was filtered, and volatiles were removed under reduced pressure. The product,  $\mathbf{1-V_6O_6Cl^{1-}}$ , was isolated as a dark brown solid (22 %, yield determined by <sup>1</sup>H NMR spectroscopy, see supporting information for details). Resonances matched values reported previously for complex  $\mathbf{1-V_6O_6Cl^{1-}}$ .<sup>39</sup>

*Synthesis of  $V_6O_6Cl(OC_2H_5)_{12}$  (**4- $V_6O_6Cl^0$** ) via chlorination of  $[V_6O_7(OC_2H_5)_{12}]$  (**3- $V_6O_7^0$** ) with  $TiCl_3(thf)_3$*

A 20 mL scintillation vial was charged with **3- $V_6O_7^0$**  (0.031 g, 0.032 mmol) and  $TiCl_3(thf)_3$  (0.015 g, 0.041 mmol). Dichloromethane (5 mL) was added, and the reaction was stirred at room temperature for 1 hour. Volatiles were removed under reduced pressure.  $^1H$  NMR analysis of the crude product revealed a mixture of products. Purification of the neutral halogenated cluster, **4- $V_6O_6Cl^0$**  was accomplished by dissolving the dark brown residue in dichloromethane and filtering the solution over silica (6 cm). Volatiles were removed under reduced pressure to obtain **4- $V_6O_6Cl^0$**  as a yellow-brown solid (0.016 g, 0.017 mmol, 52 %).

*Synthesis of  $[V_6O_6(OC_2H_5)_{12}][OTf]$  (**6- $V_6O_6OTf$** )*

A 20 mL scintillation vial was charged with **4- $V_6O_6Cl^0$**  (0.053 g, 0.054 mmol) and silver trifluoromethylsulfonate ( $AgOTf$ , 0.015 g, 0.056 mmol). Dichloromethane (10 mL) was added to the vial and the reaction mixture was stirred at room temperature for 24 hours. The resultant dark green-brown solution was filtered, and volatiles were removed under reduced pressure, affording **6- $V_6O_6OTf$**  as a green-brown solid in good yield (0.058 g, 0.051 mmol, 97 %). Crystals suitable for X-ray crystallography were grown by the slow diffusion of diethyl ether into a concentrated solution of dichloromethane.  $^1H$  NMR (400 MHz,  $CDCl_3$ )  $\delta$  = 26.57 (fwhh = 280 Hz), 12.49 (fwhh = 230 Hz), 5.85 (fwhh = 232 Hz), -0.78 (fwhh = 220 Hz), -23.09 (fwhh = 520 Hz) ppm. FT-IR (ATR,  $cm^{-1}$ ): 1028 ( $O_b-C_2H_5$ ), 980 ( $V=O_t$ ). UV-Vis ( $CH_2Cl_2$ ): 392 nm, ( $\epsilon$  = 12474  $M^{-1}cm^{-1}$ ), 1000 nm ( $\epsilon$  = 1242  $M^{-1}cm^{-1}$ ). Elemental analysis for  $C_{25}H_{60}O_{21}V_6F_3S$  (MW = 1091.44 g/mol) Calcd (%): C, 27.51; H, 5.54. Found (%): C, 27.81; H, 5.57.

*Synthesis of  $[V_6O_6Cl(OEt)_{12}][W_3Cl_5O_6(OEt)_2]$  via chlorination of  $[V_6O_7(OEt)_{12}]$  with  $WCl_6$  (**5- $V_6O_6Cl^+$** )*

A 20 mL scintillation vial was charged with **3- $V_6O_7^0$**  (0.047 g, 0.049 mmol) and  $WCl_6$  (0.028 g, 0.069 mmol). Dichloromethane (6 mL) was added, and the reaction was stirred at room temperature for 1 hour. The orange-brown solution was filtered, and volatiles were removed under reduced pressure. The orange-brown solid was stirred in 6 mL of toluene for 30 minutes. The solution was filtered and the solid was washed with toluene until it ran clear. The product was extracted with dichloromethane and volatiles were removed under reduced pressure to obtain complex **5- $V_6O_6Cl^+$**  as an orange-brown solid (0.031 g, 0.017 mmol, 41%). Crystals suitable for X-ray crystallography were grown by the slow diffusion of pentane into a concentrated solution of dichloromethane.  $^1H$  NMR (400 MHz,  $CD_2Cl_2$ )  $\delta$  = 16.49 (fwhh = 156 Hz), 10.19 (fwhh = 128 Hz), 8.51 (fwhh = 136 Hz), 3.44 (fwhh = 48 Hz), 0.77 (fwhh = 76 Hz), 0.22 (fwhh = 60 Hz), -0.57 (fwhh = 156 Hz), -21.8 (fwhh = 516 Hz) ppm. FT-IR (ATR,  $cm^{-1}$ ): 1006 ( $O_b-C_2H_5$ ), 986 ( $V=O_t$ ), 958 ( $W=O_t$ ). UV-Vis ( $CH_2Cl_2$ ): 396 nm, ( $\epsilon$  = 16700  $M^{-1}cm^{-1}$ ), 1000 nm ( $\epsilon$  = 1238  $M^{-1}cm^{-1}$ ). Elemental analysis for  $C_{28}H_{70}O_{26}V_6W_3Cl_6 \cdot C_7H_8$  (MW = 1984.85 g/mol) Calcd (%): C, 21.18; H, 3.96. Found (%): C, 21.42; H, 4.28.

## Conflicts of interest

There are no conflicts to declare.

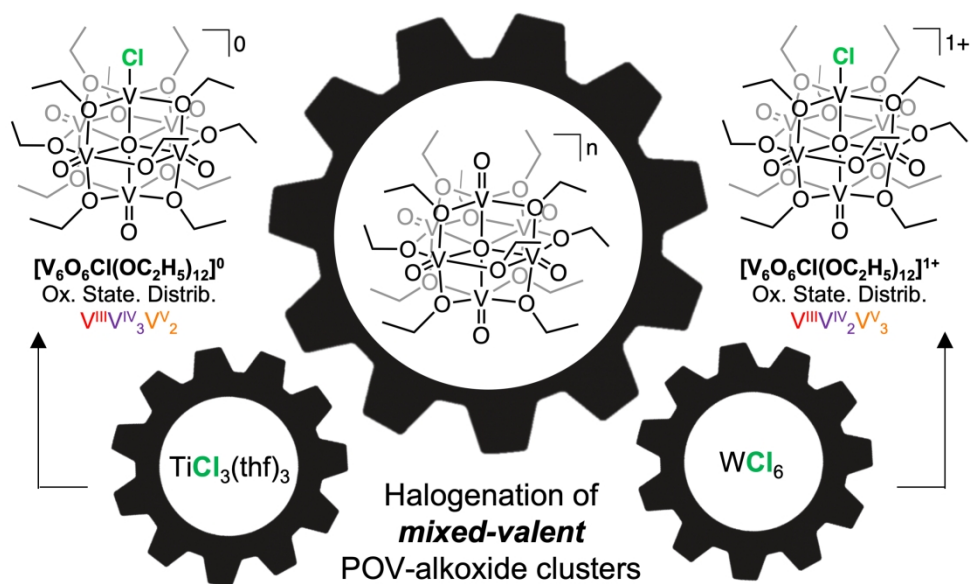
## Acknowledgements

This research was funded by the National Science Foundation through grant CHE-1653195 (M.L.M., B.E.P., and E.M.M.). The authors also acknowledge generous financial support from the University of Rochester through start-up funds.

## References

1. K. Tada, K. Sakata, S. Yamada, K. Okazaki, Y. Kitagawa, T. Kawakami, S. Yamanaka and M. Okumura, *Mol. Phys.*, 2014, **112**, 365-378.
2. Y. Ren, Z. Ma and P. G. Bruce, *Chem. Soc. Rev.*, 2012, **41**, 4909-4927.
3. D. W. Flaherty, *ACS Catal.*, 2018, **8**, 1520-1527.
4. Y. Liu, W. Wang, X. Xu, J.-P. Marcel Veder and Z. Shao, *J. Mat. Chem. A*, 2019, **7**, 7280-7300.
5. R. P. Doris Vogtenhuber, Josef Redinger, Eleonore L. D. Hebenstreit, Wilhelm Hebenstreit, and Ulrike Diebold, *Phys. Rev. B*, 2002, **65**, 125411.
6. *United States Pat.*, 3,134,732, 1964.
7. *United States Pat.*, 4,480,046, 1984.
8. *United States Pat.*, 3,201,355, 1965.
9. *United States Pat.*, 4,491,636, 1985.
10. *France Pat.*, 2,777,806A1, 1999.
11. P. K. Jena and E. A. Brocchi, *Min. Proc. Ext. Met. Rev.*, 1997, **16**, 211-237.
12. P. K. Jena, E. A. Brocchi and J. González, *Metall. Mater. Trans. B*, 2005, **36**, 195-199.
13. I. S. Pap, G. Mink, I. Bertóti, T. Székely, I. Z. Babievskaya and E. Karmazsin, *J. Therm. Anal. Calorim.*, 1989, **35**, 163-173.
14. G. Mink, I. Bertóti, C. Battistoni and T. Székely, *Reac. Kin. Mech. Catal.*, 1985, **27**, 39-45.
15. G. Mink, I. Bertóti and T. Székely, *Reac. Kin. Catal. Lett.*, 1985, **27**, 33-38.
16. R. P. Arganbright and W. F. Yates, *J. Org. Chem.*, 1962, **27**, 1205-1208.
17. K. Ebitani, Y. Hirano, J. H. Kim and A. Morikawa, *Reac. Kin. Catal. Lett.*, 1993, **51**, 351-355.
18. J. G. Weissman, E. I. Ko, P. Wynblatt and J. M. Howe, *Chem. Mater.*, 1989, **1**, 187-193.
19. B. C. Sweeny, S. G. Ard, A. A. Viggiano and N. S. Shuman, *J. Phys. Chem. A*, 2019, **123**, 4817-4824.
20. K. A. Zemski, D. R. Justes and A. W. Castleman, *J. Phys. Chem. B*, 2002, **106**, 6136-6148.
21. R. C. Bell, K. A. Zemski and A. W. Castleman, *J. Phys. Chem. A*, 1999, **103**, 1585-1591.
22. G. Pacchioni, *ChemPhysChem*, 2003, **4**, 1041-1047.
23. L. Zhang, S. Wang and C. Lu, *Anal. Chem.*, 2015, **87**, 7313-7320.
24. D. E. Katsoulis, *Chem. Rev.* 1998, **98**, 359-388.
25. D.-L. Long, R. Tsunashima and L. Cronin, *Angew. Chem. int. Ed.*, 2010, **49**, 1736-1758.
26. K. Y. Monakhov, W. Bensch and P. Kögerler, *Chem. Soc. Rev.* 2015, **44**, 8443-8483.

27. S.-M. Wang, J. Hwang and E. Kim, *J. Mat. Chem. C*, 2019, **7**, 7828-7850.
28. Y. Ren, M. Wang, X. Chen, B. Yue, and H. He, *Materials*, 2015, **8**, 1545-1567.
29. I. Efremenko and R. Neumann, *J. Am. Chem. Soc.*, 2012, **134**, 20669-20680.
30. B. E. Petel, A. A. Fertig, M. L. Maiola, W. W. Brennessel and E. M. Matson, *Inorg. Chem.*, 2019, **58**, 10462-10471.
31. B. E. Petel, W. W. Brennessel and E. M. Matson, *J Am Chem Soc*, 2018, **140**, 8424-8428.
32. F. Li, L. E. VanGelder, W. W. Brennessel and E. M. Matson, *Inorg. Chem.*, 2016, **55**, 7332-7334.
33. L. E. VanGelder, W. W. Brennessel and E. M. Matson, *Dalton Trans.*, 2018, **47**, 3698-3704.
34. R. L. Meyer, W. W. Brennessel, and E. M. Matson, *Polyhedron* 2018, **156**, 303-311.
35. M. B. Robin and P. Day, *Mixed Valence Chemistry-A Survey and Classification.*, New York, 1968.
36. C. Daniel and H. Hartl, *J. Am. Chem. Soc.* 2005, **127**, 13978-13987.
37. C. Daniel and H. Hartl, *J. Am. Chem. Soc.*, 2009, **131**, 5101-5114.
38. B. E. Petel, R. L. Meyer, W. W. Brennessel and E. M. Matson, *Chem. Sci.*, 2019, **10**, 8035-8045.
39. B. E. Petel, R. L. Meyer, M. L. Maiola, W. W. Brennessel, A. M. Müller and E. M. Matson, *J. Am. Chem. Soc.*, 2020, **142**, 1049-1056.
40. L. E. VanGelder, P. L. Forrestel, W. W. Brennessel and E. M. Matson, *Chem. Commun.* 2018, **54**, 6839-6842.
41. E. A. Pedrick, G. Wu and T. W. Hayton, *Inorg. Chem.*, 2014, **53**, 12237-12239.
42. J. J. Kiernicki, J. S. Harwood, P. E. Fanwick and S. C. Bart, *Dalton Trans.*, 2016, **45**, 3111-3119.
43. N. G. Connelly and W. E. Geiger, *Chem. Rev.* 1996, **96**, 877-910.
44. F. Li, S. H. Carpenter, R. F. Higgins, M. G. Hitt, W. W. Brennessel, M. G. Ferrier, S. K. Cary, J. S. Lezama-Pacheco, J. T. Wright, B. W. Stein, M. P. Shores, M. L. Neidig, S. A. Kozimor and E. M. Matson, *Inorg. Chem.*, 2017, **56**, 7065-7080.
45. F. Li, R. L. Meyer, S. H. Carpenter, L. E. VanGelder, A. W. Nichols, C. W. Machan, M. L. Neidig and E. M. Matson, *Chem. Sci.*, 2018, **9**, 6379-6389.
46. L. E. VanGelder, A. M. Kosswattaarachchi, P. L. Forrestel, T. R. Cook and E. M. Matson, *Chem. Sci.*, 2018, **9**, 1692-1699.
47. L. E. VanGelder and Ellen M. Matson, *J. Mat. Chem. A*, 2018, **6**, 13874-13882.
48. Q. Ren, J. Wan and Y. Gao, *J. Phys. Chem. A*, 2014, **118**, 11114-11118.
49. M.-Q. Cai, Y.-J. Zhang, Z. Yin and M.-S. Zhang, *Phys. Rev. B*, 2005, **72**, 075406.
50. S. A. Ansari, M. M. Khan, S. Kalathil, A. Nisar, J. Lee and M. H. Cho, *Nanoscale*, 2013, **5**, 9238-9246.
51. R. Asahi, T. Morikawa, T. Ohwaki, K. Aoki and Y. Taga, *Science*, 2001, **293**, 269.
52. P. D. Matthews, T. C. King and D. S. Wright, *Chem. Commun.*, 2014, **50**, 12815-12823.
53. M. Nolan, A. Iwaszuk, A. K. Lucid, J. J. Carey and M. Fronzi, *Adv. Mater.*, 2016, **28**, 5425-5446.
54. N. A. Jones, S. T. Liddle, C. Wilson and P. L. Arnold, *Organometallics*, 2007, **26**, 755-757.
55. G. M. Sheldrick, *SHELXT-2014/5*, University of Göttingen, Göttingen, Germany, 2014.
56. G. Sheldrick, *Acta Cryst. C*, 2015, **71**, 3-8.



126x76mm (600 x 600 DPI)